Experimental methods in chemical engineering

Pressure

Wu, Kaiqiao; Galli, Federico; de Tommaso, Jacopo; Patience, Gregory S.; van Ommen, J. Ruud

DOI
10.1002/cjce.24533

Publication date
2022

Document Version
Final published version

Published in
Canadian Journal of Chemical Engineering

Citation (APA)
Wu, K., Galli, F., de Tommaso, J., Patience, G. S., & van Ommen, J. R. (2022). Experimental methods in chemical engineering: Pressure. *Canadian Journal of Chemical Engineering*, *101*(1), 41-58. https://doi.org/10.1002/cjce.24533

Received: 1 March 2022 | Revised: 15 April 2022 | Accepted: 20 April 2022

DOI: 10.1002/cjce.24533

MINI-REVIEW

THE CANADIAN JOURNAL OF CHEMICAL ENGINEERING

Experimental methods in chemical engineering: Pressure

Kaiqiao Wu[1] | **Federico Galli**[2] | **Jacopo de Tommaso**[3] | **Gregory S. Patience**[3] | **J. Ruud van Ommen**[1]

[1]Product and Process Engineering, Department of Chemical Engineering, Delft University of Technology, Delft, The Netherlands

[2]Génie chimique et génie biotechnologique, Université de Sherbrooke, Québec, Canada

[3]Chemical Engineering, Polytechnique Montréal, Québec, Canada

Correspondence
J. Ruud van Ommen, Product and Process Engineering, Department of Chemical Engineering, Delft University of Technology, Van der Maasweg 9, 2629 HZ, Delft, The Netherlands.
Email: j.r.vanommen@tudelft.nl

Abstract

Pressure and temperature are the most important state variables for monitoring physicochemical processes to detect deviations that might lead to explosions and to verify levels, flow rate, and solids/gas hold-up. Pressure fluctuations in multi-phase systems identify regime changes and flow anomalies. Pressure signals are the first indicator of a process upset and are tied into distributed control systems (DCS) to sound alarms when they drift to high or low and activate safety interlocks in the case of high, high-high, low, and low-low conditions. To maximize the information, it requires that pressure gauges (transducers) are installed and calibrated precisely. Pressure measuring devices include manometers, aneroid devices like bellows and Bourdon gauges, and electronic instruments—piezoresistive, piezoelectric, and capacitive. The electronic elements have the advantage of higher precision and faster response times to measure fluctuations. The Bourdon gauges are standard equipment for pressure regulators and are mounted on the exterior of vessels and pipes to facilitate visual inspections. Over 2 million articles indexed by the Web of Science Core collection mention pressure, and in 2021, chemical engineering ranks had over 7000 articles—only multidisciplinary material sciences and energy and fuels had more. A bibliometric analysis identified five research clusters: temperature, combustion, and kinetics; separation, membranes, and energy efficiency; carbon dioxide (capture and storage), water, and thermodynamics; methane, adsorption, and transport phenomena (e.g., diffusion and permeability); and modelling, optimization, and computational fluid dynamics (CFD).

KEYWORDS

bourdon gauge, chaos theory, Hurst analysis, Nyquist criterion, pressure

1 | INTRODUCTION

The chemical industry measures temperature and pressure more than any other variable in production facilities as it reflects its state and performance. It is a strategic requirement throughout all stages of online process supervision, safe operation, efficient production, and quality control. Simple applications include a set-point comparison to maintain a sufficient holdup of gas or liquid, continuous monitoring for flow rate (e.g., orifice and venturi meters), periodic monitoring to evaluate changes in composition, continuous sampling to control unit processes,[1] and part of a comprehensive safety interlocks. In parallel, many techniques, developed

primarily for medical analysis and fluid mechanics, have been applied to inspect and quantify the hydrodynamics of gas–solid suspensions in a laboratory unit. Modern pressure measurement is routine, robust, inexpensive, and easy to integrate. The instrumentation consists of a sensing component that is in contact with the process at which pressure changes, a transducer that translates the sensed variations into measurable signals, and transmitters that relay the signal to a distributed control system that records and displays the information. Advances in digital technology have decreased costs and size while reducing instrument cost. For example, an analyst plugs and plays a mug-sized, portable electric sensor and quickly obtains the pressure readouts from the digital display. When measuring pressure in a reactor, an electronic pressure sensor is connected to a short hose with one end flushed to the nozzle, usually on the inner wall to avoid fluid invasion. Several pressure sensors probing at various heights along the vessel provide a certain redundancy and assures that the signal is meaningful.

Pressure sensors available in the market satisfy the measurement conditions of most applications. Specially designed models and electric sensors can withstand extremely high temperature, reactive conditions, and a wide measuring scale, ranging from a few millibars to a 1000 bars. Nevertheless, the growing variety of pressure sensors and the sophistication of electronics also complicate the selection and set-up of instrumentation. Unsuitable sensor types lead to unreliable pressure measurement. Interpreting pressure fluctuation is nontrivial.[2] Mapping measured pressure signals to corresponding hydrodynamic events requires a strong prior knowledge, and a proper selection of analysis methods to decompose and extract essential characteristics.

This tutorial review focuses on pressure fluctuation in gas–solid fluidized reactors. We introduce various pressure sensors and discuss the analysis methods and how to implement them. We also describe the common sources of errors and relevant troubleshooting. This work belongs to the series of articles dedicated to experimental methods in chemical engineering.[3] The goal is to introduce early-career researchers and engineers to the fundamentals of pressure measurement and provide a document that establishes a rational to design, collect, and interpret the data and assess its accuracy and reliability.

2 | THEORY

In addition to monitoring time-averaged pressure to characterize operational stability, measuring pressure fluctuations at a frequency greater than 100 provides insights into the hydrodynamic characteristics of systems. These characteristics relate to global and local events such as bubble coalescence and breakup, mass oscillations, shock waves, and even downstream perturbations introduced through blowbacks on filters.[4]

2.1 | Type of pressure measurement

Instruments measure absolute, gauge, and differential pressure (Figure 1). Absolute pressure expresses the difference between the measured pressure and absolute zero. We refer to this absolute pressure for low-pressure systems, for vacuum, aircraft applications, and near atmospheric operations. Gauge pressure is the difference between the measured and local atmospheric pressure (Equation (1)). The atmospheric pressure is dependent on geographic location, altitude, as well as ambient conditions.

$$P_g = P_{\text{measurement}} - P_{\text{atm}} \tag{1}$$

Differential pressure—difference between the pressure at two distant locations—can either be negative or positive:

$$\Delta P = P_2 - P_1 \tag{2}$$

2.2 | Pressure sensors

Devices are designed for sensing pressures up to 700 MPa. Material deformation and changes in resistance (or other electrical properties) are the fundamental properties that correlate with the pressure that a gauge measures.[6]

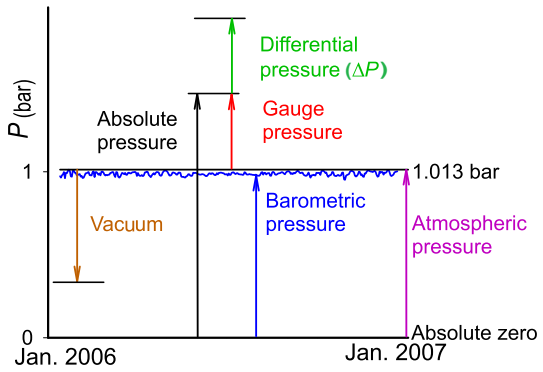

FIGURE 1 Types of pressure. The blue line represents the ambient pressure in Montreal in 2006. Barometric pressure changed by as much as 3% in 2 days, and the maximum and minimum pressures during the year were 1.0129 and 0.9519 bar, respectively. Adapted from Patience.[5] Copyright Elsevier, 2017

Pressure gauges and electrical transducer (or transmitter) are the two categories of sensors. Gauges are mechanical devices that produce an analogue visual signal and include those that measure hydrostatic head (U-shaped manometers), and aneroid gauges like bellows and Bourdon tubes that deform elastically. Manometers function based on the communicating vessels principle: an imposed pressure on one side results in a net pressure difference between two arms, driving a displacement of the reference liquid (usually mercury or water) on the display tubes until a new balance is reached. The difference in heights Δh between the two columns is proportional to the pressure and density of the liquid ρ_{liq}, and communicating fluid, ρ_{fluid}

$$\Delta P = \left(\rho_{liq} - \rho_{fluid}\right) g \Delta h \tag{3}$$

These simple instruments are best suited for laboratories and as calibration standards for electrical sensors.

The McLeod gauge, to assess pressure down to 0.1 Pa, also depends on the height difference in two columns.[5,7] Low-pressure gas (P_1, which the unknown variable), is trapped in a bulb with a known volume (e.g., V_1 = 15 ml). Mercury pumped into the bulb compresses the gas into a calibrated capillary tube at the top of the bulb with tick marks along the side to indicate volume (V_2) and height. According to Boyle's law,

$$P_2 V_2 = P_1 V_1 \tag{4}$$

The height difference (Δh) between the empty space in the capillary and an adjoining stem equals P_2, and so rearranging Equation (4), we calculate P_1. This device is best for non-condensable gases as it underestimates pressure for vapours prone to condensation. Manometers are susceptible to errors introduced by mechanical vibration and reading the height of the meniscus.[8]

Deadweight testers (piston gauges or pressure balances), is a type of null meter wherein the pressure exerted by the fluid beneath the piston is balanced by supplying weights to the level platform, acting as a downward force, until the reference mark is reached. Due to the large cross-section, the accuracy of deadweight gauges reaches ±0.01%. This gauge is mainly applied to calibrate mid-range instruments.

Aneroid gauges evaluate pressure with metallic materials that deform elastically under a load. For bellows, the external pressure induces a translational expansion at the other end of the device (Figure 2A). Bourdon tubes consist of a specially shaped hollow tube, which is fixed at one side and free to rotate at the other end. The shapes include C-type, spirals, and helices. The deflection of the tube is proportional to the imposed pressure (Figure 2B).

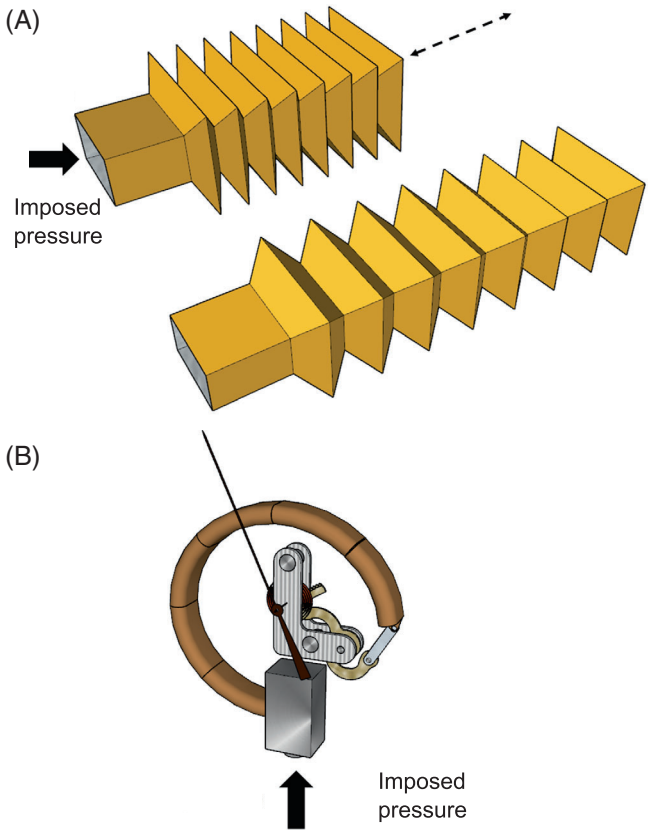

FIGURE 2 Mechanical (aneroid) pressure gauges: (A) the bellows and (B) the C-shaped bourdon tube

These devices are installed on regulators, vessels, and pipes to facilitate visual inspections.

Another type of aneroid gauge comprises a thin pressure- sensing diaphragm, which deforms under in proportion to the pressure difference between the two sides. One side communicates with the high pressure while the other side is connected to downstream of the system to read ΔP or to atmosphere to give P_{gauge}. The metallic, ceramic, or silicon diaphragms are either thin flat plates, corrugated disks, or membranes, depending on the thickness and the magnitude of the pressure. Metallic diaphragms withstand high and burst pressure, whereas ceramic types are good for corrosive environments. The gauge factor of silicon is greater than the metallic type. The diaphragms deflection, y is proportional to the pressure drop, the radius of the disk to the fourth power, r, and inversely proportional to Young's modulus, E_Y, and the thickness cubed, t,

$$y = \frac{3\Delta P}{16 E_Y t^3} r^4 \left(1 - \nu^2\right), \tag{5}$$

where ν is the Poisson's ratio.

2.2.1 | Electronic pressure sensors

Diaphragm gauges (transducers) respond quickly to pressure fluctuations and are ideal as the sensing element in electronic pressure sensors and calibration instruments (Table 1). These electronic sensors translate deflection induced by ΔP into an electrical signal. Compared to pressure gauges, they are more convenient and are preferred for data acquisition modules, automatic control systems, safety interlocks, or to monitor systems with rapid pressure fluctuation. The sensors output either voltage or current. Millivolt (mV) output transducers are less expensive and have electronics to passively trigger a low electrical output of the Wheatstone bridge without amplification and filtering. The full-scale output signal of a millivolt-type transducer is directly proportional to the power supply alongside a sensitivity of a few millivolts per volt. Subsequently, the output is relatively low in magnitude and also varies if the excitation fluctuates. Compared to other electronic sensors, millivolt transducers excel with a very fast response and the lowest power consumption, which is ideal to measure fast dynamic applications. Owing to the low output amplitude, millivolt-output transducers are preferred in a noise-free environment,[9] and a regulated, robust power supply is required to stabilize the output. Short signal wires minimize the voltage attenuation due to the wire resistance (3–6 m).[10] Voltage-output transducers include onboard amplification modules to boost the Wheatstone bridge output, that is, 5–30 V, and minimize the electromagnetic interference (EMI), which relaxes the restriction of short wires. A lower-cost unregulated supply module is sufficient to drive the device. Pressure transmitters, in contrast, output a current signal of a magnitude of milliamps (mA). They are normally designed to deliver an output current of 4–20 mA, which plugs onto industrial sensing and control circuits. At this current, EMI is negligible, so signal wires can be extended to several hundred meters, ideal for long-distance communication. Omega recommends powering pressure transmitters through the electric grid rather with batteries.[11]

2.2.2 | Electronic sensing principle

The electronic elements' quality is paramount to measure pressure accurately, reliably, with a broad range, and compatible with the system environment. Piezoresistive, piezoelectric, and capacitive signal-converting elements dominate the market. Piezoresistive elements stretch with applied pressure that induces variations in the electrical resistance of one or more mounted resistors (Figure 3A). The resistance varies linearly with the diaphragm. The resistors are integrated onto a Wheatstone bridge circuit powered by an excitation voltage. All the resistors connected to the bridge are balanced without strain, resulting in a null voltage output. Small resistance variations unbalance the bridge and create an output from the circuit.

Piezoresistive pressure sensors are highly sensitive, robust, and thermally resistant. The inherent frequency of the piezoelectric pressure sensors is up to several hundred kHz, which renders them suitable for measuring fast-varying signals.[12] The output is also stable over time. Piezoelectric sensors are robust to electromagnetic noise, inexpensive, and consume little power. For a piezoelectric sensor, the pressure exerts a force on an element fabricated with a piezoelectric crystal material, such as quartz and ceramic, thus producing a voltage across it. The output is proportional to the downward pressing force that displaces (Figure 3B). The sensing elements are rigid, thermally resistant, respond on the order of microseconds and operate from 0.07 to 70 000 ka with an accuracy of ±1%. However, the output signal is relatively weak, and they are

TABLE 1 Comparison of transducer and transmitters properties

Millivolt transducer	Voltage transducer	Transmitter	
Noise susceptibility	Very sensitive to noise	Less susceptive to noise	Low susceptibility to noise
Communication distance	Short distance (3–6)	Medium distance (30)	Long distance (300 or more).
Power consumption	Less power consumption	Lower power consumption than pressure transmitter	Higher power consumption than transducers
Excitation voltage	Stable bridge-excitation voltage is required	Unregulated bridge-excitation voltage is sufficient	Unregulated bridge-excitation voltage is sufficient

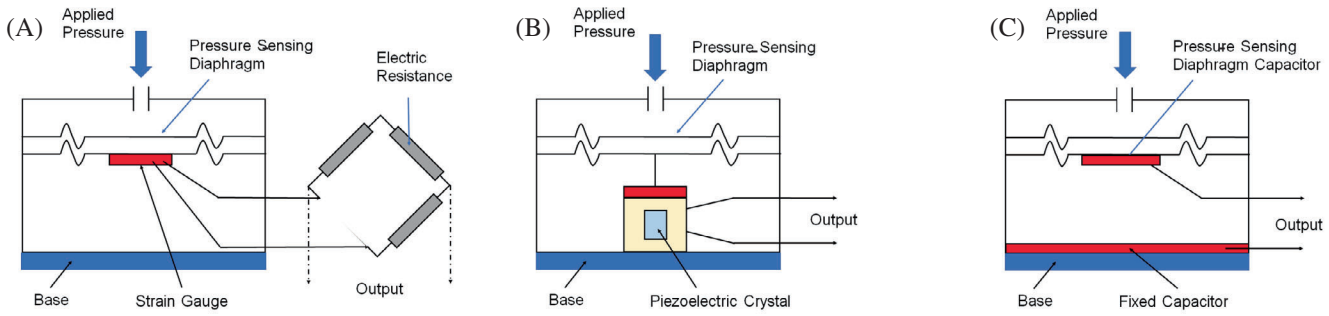

FIGURE 3 Schematic of pressure transducers: (A) strain gauge, (B) piezoelectric crystal, and (C) fixed capacitor

less accurate than piezoresistive sensors. Furthermore, a compensation module is always required to mitigate vibration or acceleration.

Capacitive pressure sensors measure changes in electrical capacitance caused by the strain of the diaphragm, which functions as one of the electrodes (Figure 3C). Under an exerted pressure, the diaphragm deforms that changes the capacitance of the circuit. These sensors are accurate, sensitive, and apply from 0.2 to 70 000 Pa. They resist high-pressure pulses of a 1000 times the rated full-scale pressure.[8] Therefore, they are effective for low-pressure measurement and harsh environments. As no direct current (DC) is produced through the capacitor, they are inherently low in power consumption. The response time is in the order of milliseconds with low hysteresis. The output depends on the gap between the parallel electrode plates, therefore unsuitable for applications that vibrate. In addition, diaphragm deformation can also be monitored via the use of an optical emitter-detector coupler (fibre-optic sensors), or inductive reluctance (e.g., magnetic pressure transducers).

Other types of sensors, such as thermal sensors, ionization sensors and resonant wires, are designed for specific measurements, in which a high order of accuracy or extreme pressures are the primary consideration.[6]

2.3 | Origin of pressure fluctuation

Pressure fluctuations indirectly reflect local and global hydrodynamics of a gas–solid mixture. Decomposing pressure fluctuations and associating each segment with underpinning events require an understanding of the system hydrodynamics. Nevertheless, due to its complexity, there is yet not a clear consensus on the origin of pressure fluctuations. A time series of pressure fluctuation reflects both local fluctuations caused mainly via bubble propagation and global compression waves induced by a variety of hydrodynamic events.

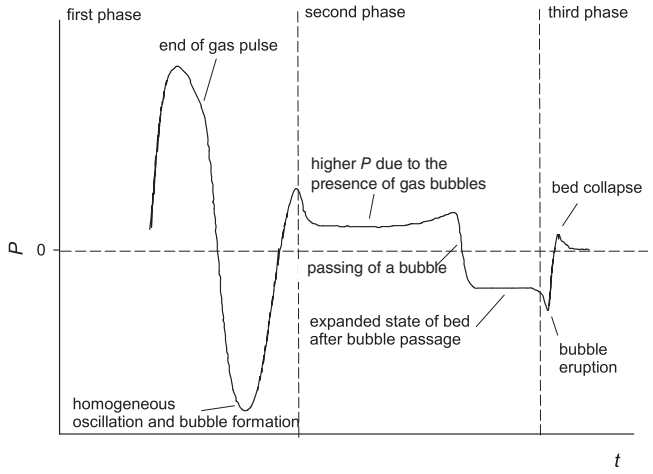

FIGURE 4 Plenum pressure response due to a gas pulse injection. Adapted from van der Schaaf[15] Copyright Elsevier, 1998

2.3.1 | Local events

Upward rising bubbles alter the gas stream and perturb the pressure signal of probes in the vicinity according to the Davidson model,[13,14] for an infinitely wide column. Van der Schaaf et al.[15] monitored pressure fluctuations in a finite column ($D < 10$ cm) operating at the minimum fluidization velocity (U_{mf}) after injecting a pulse of gas to the plenum. They identified three phenomena as the bubble passed a probe in the bed: the nucleation, propagation, and rupture (Figure 4).

During the first phase, particles are motivated by the increased gas flow rate, and the bed compresses, thus decreasing voidage. The pressure reaches a maximum at which interphase friction peaks. The particulate bed then starts to expand and interphase friction decreases correspondingly, which decreases the pressure signal. Particles carrying inertia continuously rise and dilate. At its largest dilation, where the bed is about to contract, it reaches a minimum. During the second phase, a large bubble is nucleated from the distributor plate. A significant bed mass is lifted and suspended over the probe nozzle due to

the presence of rising bubbles. This reflects the enduring pressure occurring at the beginning of the second phase. When the bubble travels by the probes, pressure recovers but remains slightly less than that in the pre-pulsed state, as the particulate phase is still under an expansion state with higher voidage than the minimum fluidization. Rising further through the bed, the bubble ruptures at the bed surface in the third phase, and the excited state collapses from the lower section after the bubble passes by (Figure 5). The excited bed eventually recovers to a steady fluidization state after contracting.[16]

2.3.2 | Global events

Hydrodynamic events drive the compression of solids and create fast-travelling waves inside the column that propagate upwards and downwards. In a relatively small column, an ascending wave decays linearly through the bed, whereas a descending wave maintains its intensity.[15] Sources of compression waves are due to step-change bubbling events, such as bubble formation, coalescence, and breakup. Bubble formation at the distributor plate pushes particles upwards and initializes a corresponding peak in the pressure signal. The major pressure fluctuations are in line with the characteristic bubbling frequency.[17] Bubble coalescence creates waves in both the upwards and downwards directions but are more pronounced in the lower section of the bed.[18] Fluctuations in gas flow are strongly linked with bubble events, where gas streams utilize rising bubbles as shortcuts to channel to the bed surface, resulting in an inhomogeneous flow rate distribution.[15] Such a coupling

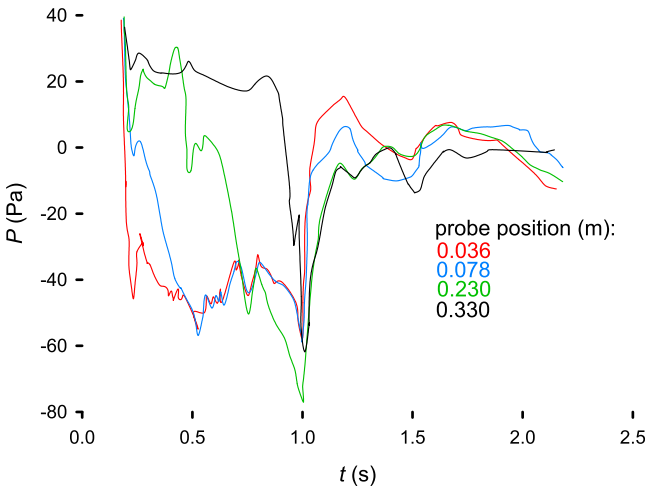

FIGURE 5 Pressure response after a sudden gas pulse injection to a fluidized bed plenum operating at U_{mf}. Reprinted with permission from van der Schaaf et al.[15] Copyright Elsevier, 1998

develops spatio-temporally with bubbles and is less predictable. Nevertheless, part of the pressure fluctuations is associated with oscillation of bed mass around the measuring probe, which is induced alongside bubbling phenomena.

2.4 | Methods of analysis

Pressure fluctuations are monitored and stored as time-averaged and time-resolved signals. Time-averaged pressure signals in commercial units provide a means to supervise the process and identify changes with time.[19] The average bulk density, ρ_{bulk}, the quotient of the time-averaged pressure difference, ΔP and the difference in height between two sensors, h (neglecting fluid density, acceleration, and other forces):

$$\rho_{bulk} = \frac{\Delta P}{gh} \tag{6}$$

When the bulk density is known and the suspension is homogenously dispersed, we apply Equation (6) to determine the bed expansion. When the pressure is sampled at a sufficiently high frequency, the time-resolved pressure fluctuation is more insightful into hydrodynamics. Van Ommen et al.[20] deciphered 1D signal of pressure fluctuation of various bed regimes.[21] The pressure fluctuations were collected in a 10 × 70 cm riser of a circulating fluidized bed of Geldart B silica sand particles ($d_p = 320$ μm). The particulate medium was fluidized at four superficial gas velocities to achieve various bubbling states. The probes were mounted at 20 cm above the gas distributor plate. They applied time, frequency, and state analyses of pressure.

2.4.1 | Time domain analysis

In comparison to other approaches, analysis in the time domain is intuitive. We recommend plotting the raw measured pressure signals against time and calculating standard deviation or variance. Both relative and absolute expressions yield similar trends. Standard deviation correlates with fluidization quality, which reflects the evolution of particle size,[20] bubbles in beds of a different diameter,[22] and different assisted methods.[23] A change in standard deviation corresponds to in fluidization regime and flow patterns,[24] such as transitions between sub-fluidization and fluidization states,[25-27] as well as from bubbling to turbulent fluidization.[21,28-30] However, the standard deviation is associated with the distribution of bulk density, which is a function of superficial gas

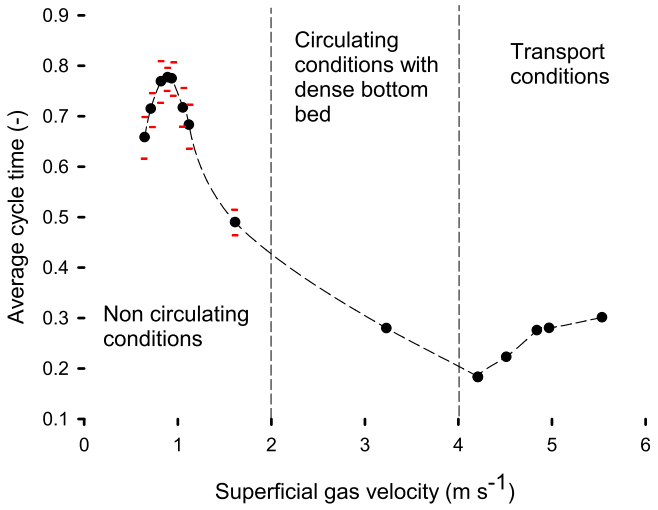

FIGURE 6 The average cycle time as a function of the superficial gas velocity. Red horizontal bars represent 1 σ and when absent, the symbol is larger than the error. Adapted from van Ommen et al.[20]

velocity. Moreover, in most large units, the gas supply varies.

The average cycle time (ACT) is another useful attribute that records the number of times a pressure signal crosses its arithmetic mean. Figure 6 demonstrates clearly distinguished trends of ACT across several fluidization regimes. Within the same fluidization regime (e.g., the bubbling regime), ACT is independent of gas velocity, static bed loading, and particle size in simulated systems.[31] Van Ommen et al.[25] also suggested that ACT varies with particle agglomeration inside the bed. ACT is susceptible to noise—rapid oscillations around the mean—so we apply a low-pass filter, which attenuates all the signals at frequencies higher than a certain cut-off frequency[32] or a Hurst analysis, which assists in determining the optimal timestep to exclude stochastic components from the signals.

2.4.2 | Frequency domain analysis

A time series of the pressure signal is more commonly studied in the frequency domain by Fourier-transform analysis, which converts time-series to spectral profiles. Spectral analysis identifies the oscillation frequencies present in the pressure fluctuations and correlates them with physical phenomena. For non-parametric analysis, a decent number of sub-spectra is first computed from the segments of a long time-series signal by Fast-Fourier transformation (FFT). In order to smooth out noise, the final output spectrum is computed as the average of the sub-spectra. A good trade-off between segment length and deviation needs to be considered.[21] Figure 7 shows Bode plots of the power spectra of four bubbling regimes.

The experiments demonstrate that it is reasonable to depict pressure fluctuation of bubbling beds as a set of second-order oscillators.[20] For the single- and the exploding-bubble regime, systems behave similarly to pronounced, underdamped oscillators, with clear peaks at the dominant bubbling frequencies. On the other hand, the system in the multiple-bubble regime behaves as an underdamped system of a higher damping factor, with a broader mode at frequencies of 20–40 rad s^{-1}. When entering the transport regime, the damping is stronger. Its bode plot can be approximated using straight asymptotes for low- and high-frequency regions.

Alternatively, the fluctuations in pressure signals can be investigated by plotting transient power spectral density. Compared to overall power spectra, it shows the temporal evolution of hydrodynamics events occurring at different frequencies. Similarly, sub-spectrum is also first computed based on segments of a long time series by FFT. The power density is evaluated over the entire time sequence (Figure 8). For all the bubbling regimes, bubbling events mainly spread below 5 Hz. Both the single-bubble regime and exploding-bubble regime have a single dominant frequency at 1.2 Hz, and it is fairly stable over time. In contrast, there is no dominant frequency observed for the multiple-bubble scenario.

This method provides an effective way to monitor temporal changes in the oscillation mode of a fluidization regime. Transient power spectral density is unable to capture events in the time scale of seconds, and additional consideration is required in selecting a suitable number of segments. There are more advanced frequency analysis methods, such as wavelet methods to decompose pressure signals, providing additional insights.[20]

2.4.3 | State domain analysis

Applying the techniques in chaos analysis opens a new avenue to look into system hydrodynamics. A fluidized system was considered as a chaotic system from a mathematical point of view,[37] although this remains debatable. In the late 1990s, researchers applied chaos to pressure fluctuations and state-space analysis.[38] A transient state of fluidization could be characterized by mapping governing variables to a multidimensional space, that is, the state space. The trajectory of temporal evaluation of the system state is an 'attractor'. Since it is impractical to pinpoint and track all the governing variables of a complex multiphase system, the attractor, we reconstruct it from the time series of a single

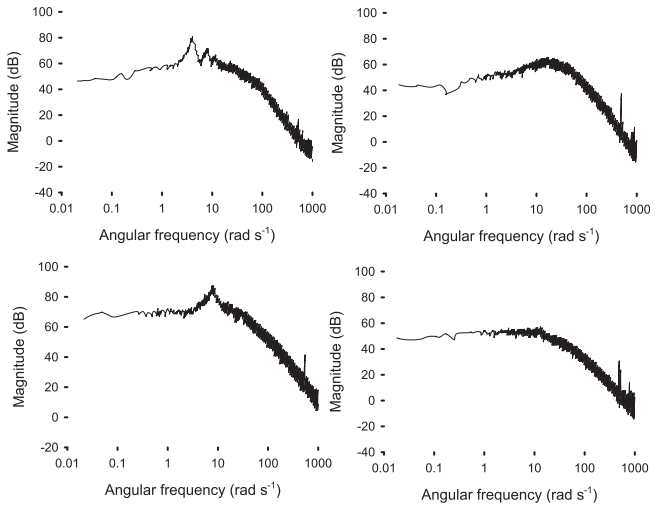

FIGURE 7 Bode plots for the four fluidization regimes, reprinted with permission.[20] Copyright Elsevier, 2011

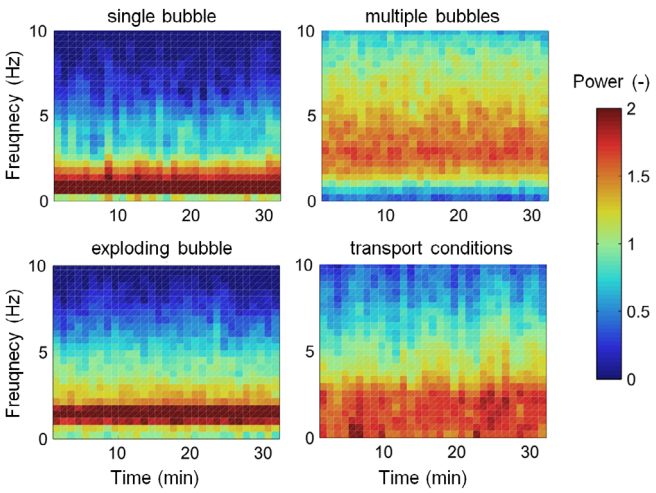

FIGURE 8 The transient spectral density for the four selected cases, applied to normalized pressure signals. Colours represent power intensity. Reprinted from van Ommen et al.[20] with permission. Copyright Elsevier, 2011

characteristic variable of the system.[39] In the time-delay coordinates, a normalized pressure series of n values (P_1, P_2, P_3, ..., p_n) is first converted into a set of $n-m$ delay vectors P_k with m elements, which is the embedding dimension. Van Ommen et al.[20] suggested that an embedding dimension on the order of 10 is sufficient to represent attractors. Figure 9 illustrates the attractors as an assembly of the successive system states, with an embedding dimension of two. The attractors exhibit different structures in the embedding domain and function as 'fingerprints' of the system dynamics.

Kolmogorov entropy, a feature extracted attractor reconstruction characterizes the rate of information lost. Schouten et al. proposed a procedure to calculate the maximum likelihood estimate of the Kolmogorov entropy from experimental time-series.[40] It follows pairs of closely located points on the attractors that are closer than a threshold length scale until the paths diverge to a distance greater than the threshold. A linear system has a predictable entropy of zero, whereas a stochastic system is unpredictable in time.

3 | APPLICATIONS

The Web of Science (Wos) has indexed over 2 million articles that appear when selecting pressure as the search criteria Topic.[41] The other physical quantities that occur often include: time (8.8 million), temperature (4 million), flow (2.5 million), and mass (2.4 million). Multidisciplinary material sciences cites pressure most of the over 250 scientific categories in Wos with over 166 000, followed by applied physics (129 000), and mechanical engineering (122 000). Chemical engineering ranks fourth with 120 000 occurrences. The top cited article 'Gender Difference in the Relationship Between Lipid Accumulation Product Index and Pulse Pressure in Nondiabetic Korean Adults: The Korean National Health and Nutrition Examination Survey 2013-2014' in 2021 accrued 2231 as of February 2022. (The article appeared in print in February 2022 but was available with early access in November 2021.)

We created a bibliometric keyword map based on the 7000 articles in journals that WoS assigned to chemical engineering. The VOSViewer open-access software created five clusters of the 100 keywords that occur most often and grouped them according to how often they appear together (Figure 10). They also have created links between keywords based on citations in the articles. The red cluster has 32 keywords, and the main themes are combustion, kinetics, and temperature. The green cluster has the second most number of keywords at 21 and deals with separation, membranes, desalination, and energy efficiency. The major theme of the blue cluster, with 18 keywords, is CO_2, thermodynamics, and liquid systems. The yellow cluster (18 keywords) is more dispersed in the map and is centred on CH_4 and mass transfer phenomena like adsorption, permeability, and diffusion. The magenta cluster (17 keywords) is devoted to modelling—CFD, hydrodynamics, design, and optimization.

In 2021, *Fuel, Energy & Fuels*, and *Chemical Engineering Journal* each published 697, 394, and 335, which is expected since they rank 2, 9, and 1, respectively, in terms of the number of articles published in 2021. *The Canadian Journal of Chemical Engineering* published 69 articles that mention pressure. The cited articles were

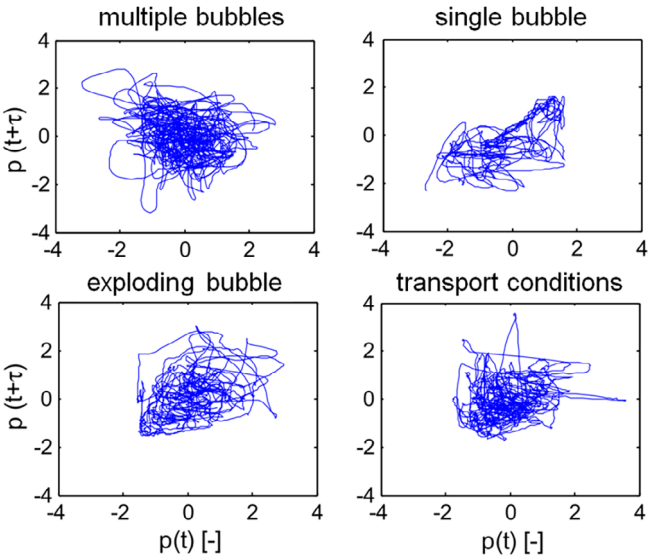

FIGURE 9 Two-dimensional attractors of various bubbling conditions, obtained with an embedded dimension of two. Reproduced from van Ommen et al.[20] Copyright Elsevier, 2011

'Guidelines for Performing Lignin-First Biorefining'[43] (65 citations, red cluster), 'Anti-Freezing, Resilient and Tough Hydrogels for Sensitive and Large-Range Strain and Pressure Sensors',[44] (52 citations), and 'An Overview of Inorganic Particulate Matter Emission from Coal/Biomass/MSW Combustion: Sampling and Measurement, Formation, Distribution, Inorganic Composition and Influencing Factors',[45] (51 citations, red cluster). The three top cited articles in *The Canadian Journal of Chemical Engineering* were 'Liquid Film Thickness of Two-Phase Slug Flows in Capillary Microchannels: A Review Paper' (magenta cluster),[46] 'An Insight Into the Formation of Liquid Bridge and Its Role on Fracture Capillary Pressure During Gravity Drainage in Fractured Porous Media' (yellow cluster),[47] and 'Computational Fluid Dynamic Simulations of Regular Bubble Patterns in Pulsed Fluidized Beds Using a Two-Fluid Model' (magenta cluster).[48]

Applications of pressure measurement vary from routine set-point monitoring to a more complex analysis of fluctuation characteristics for system control (blue cluster). Pressure fluctuations have been analyzed to reflect the quality of fluidization (magenta cluster but below the threshold of 58 articles). We monitor bubbling events in columns to characterize mixing and heat/mass transfer (magenta cluster). Van der Schaaf et al. estimated the bubble properties via probing the standard deviation of the local pressure fluctuations at different heights using a 385 mm diameter bubbling fluidized bed of Geldart B sand particles.[49] The deviation caused by gas bubbles rising is proportional to the characteristic length scale of bubbles at the height of measurement (Figure 11); therefore, it is reflected in the pressure signal perturbation. The authors proposed that the average bubble diameter D_b was proportional to the standard deviation, σ_{xy}, and inversely proportional to the solid density, ρ_S, and voidage at minimum fluidization, ϵ_{mf},

$$D_b \sim \frac{\sigma_{xy}}{\rho_S g(1-\epsilon_{mf})} \tag{7}$$

The calculated bubble size correlates with the superficial velocity and the Darton model.[50]

Furthermore, bubbling events correlate with the pressure fluctuation power spectrum. The high-intensity power spectrum is in the low-frequency regime, (1–10 Hz), in which the local bubbling events are present (Figure 12).

Pressure fluctuations increase with gas velocity and bubble size. Van Ommen et al.[25] applied standard deviation to identify defluidization. In a pilot-scale 384 mm diameter column, when U_g dropped from 0.13 to 0.03 ms^{-1}, the standard deviation reached a minimum at ($t = 50$ s), whereas the pressure drop remained constant for another 100 s (Figure 13). Changes in $\sigma_{x,y}$ correlate with flow regime transitions. Nevertheless, its dependence on the gas velocity complicates the analysis in industrial applications, where gas velocity varies with time.[20,51] However, a peak in the standard deviation that occurs at increasing gas velocity is considered the onset of the turbulent regime.[12,28]

Fluidizing Geldart B type glass particles in 100 mm square bed, Xiang et al.[52] observed that the change in Kolmogorov entropy also reflects the transition from a mild fluidization state to a violent oscillation state. The dominant frequency of pressure fluctuations depended on the static bed height, but barely changed with the gas velocity when it reached 0.2 ms^{-1}. State analysis is also valuable to monitor the alteration in particle size distribution. Bartels et al. applied the attractor comparison in different pilot-scale circulating fluidized bed reactors and demonstrated that the attractor comparison is generally sensitive to minor changes in particle size.[53] Depending on the measurement positions and bed configuration (L-valve or loop seal), the comparison could recognize a lower than 5% change in the size of 235 μm particle. The method, with a low-pass filter, is robust to the hold-up change, up to 20%. The standard deviation correlates with the characteristic size of the particles. Within the same flow regime, Davies et al.[54] observed a linear correlation between the standard deviation and gas velocity, which is also associated with the particle size. This provides a potential for online monitoring of particle size change. Measurement pressure predict minimum fluidization

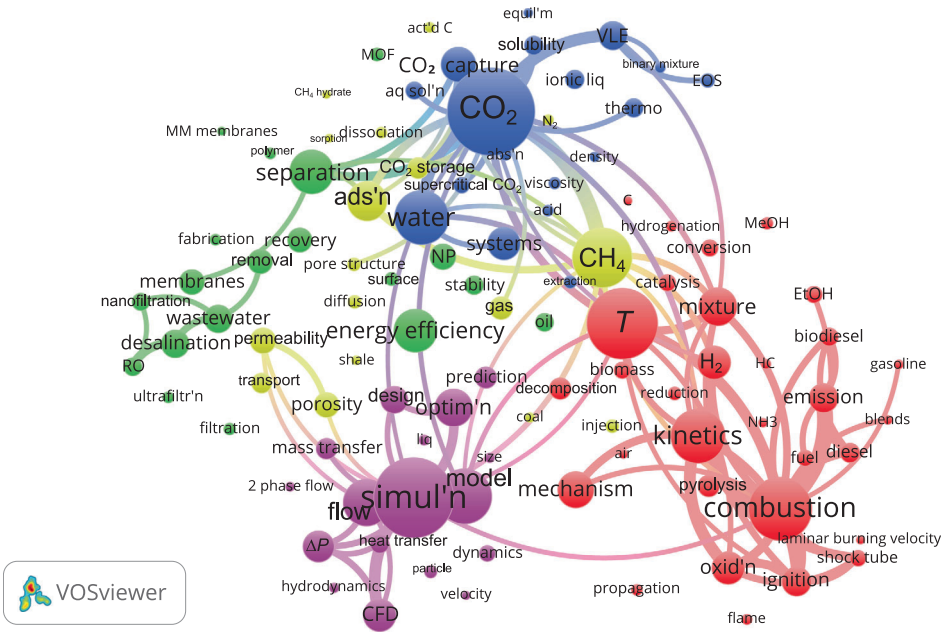

FIGURE 10 Bibliometric map of the 100 keywords that occur most often in the 7000 journal articles Web of Science (WoS) assigned to chemical engineering in 2021.[41,42] The font size and circle size represent the number of articles the keywords appear in, and the colour represents co-occurrences in the articles. The largest circle is CO_2, and it is in 568 articles, while the smallest circles correspond to 59 articles. Temperature (T) (red)—Appears in 457 articles and the cluster has 32 keywords; separation (green)—285 articles, 21 keywords; CO_2 (blue)—568 articles, 18 keywords; CH_4—386 articles, 18 keywords; and, simulation—516 articles, 17 keywords. We excluded pressure (red cluster) from the map with 783 occurrences as the size of the circle would dwarf and overlap the others too much. Performance, chemistry, behaviour, impact, and parameters were also excluded. abs'n, absorption. act'd C, activated carbon. ads'n, adsorption. aq sol'n, aqueous solution. C, carbon. CFD, computational fluid dynamics. EOS, equation of state. equil'm, equilibrium. HC, hydrocarbon. liq, liquid. MM membranes, mixed media membranes. MOF, metal organic framework. nanofiltr'n, nanofiltration. NP, nanoparticle; optim'n, optimization; oxid'n, oxidation; RO, reverse osmosis; simul'n, simulation; T, temperature; VLE, vapour–liquid equilibrium

velocity and bubbling fluidization velocity.[49,55,56] Analyzing the pressure signals generated over time, van der Schaaf et al. demonstrated that the Kolmogorov entropy calculated at a specific length scale is directly proportional to the characteristic frequency of fluidized beds, with evidence from several time series in bubbling, slugging, and circulating fluidized beds.[57] They also showed the dependence between entropy and characteristic frequency, therefore the bubble eruption frequency. Limited validation in industrial installations/pilot scales: most complex analysis methods have been tested extensively in laboratory-scale units only. Their validation is unknown for industrial installations.[58]

Pressure measurements are valuable in other applications and are typically used for monitoring purposes and trouble-shooting. For example, pressure signals determine liquid levels in reservoirs. Pressure measurement also assists in detecting potential pipe leaks and ruptures. Using one or multiple differential pressure sensors to isolate different segments of a pipe and determine the precise locations of leakage, at which there is an abnormally significant pressure drop. Differential pressure correlates with flow rate through orifices and porous media.

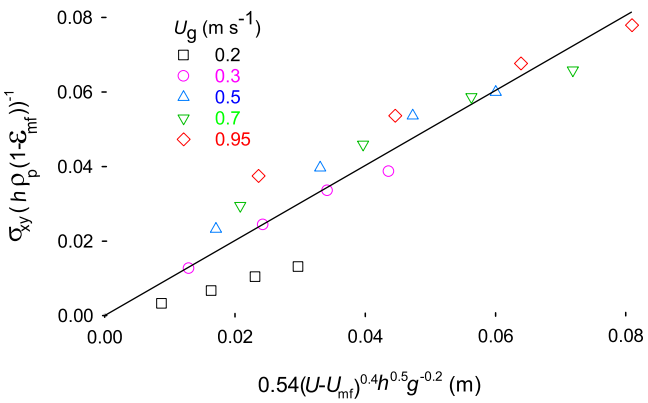

FIGURE 11 The characteristic length scale from the standard deviation versus the predicted bubble diameter predicted (Equation (7)) Adapted from van der Schaaf et al.[49]

4 | UNCERTAINTY, Δ_P

4.1 | Measurements guidance

Prior to collecting data, measure pressure long enough and at a sufficiently high frequency to ensure it is

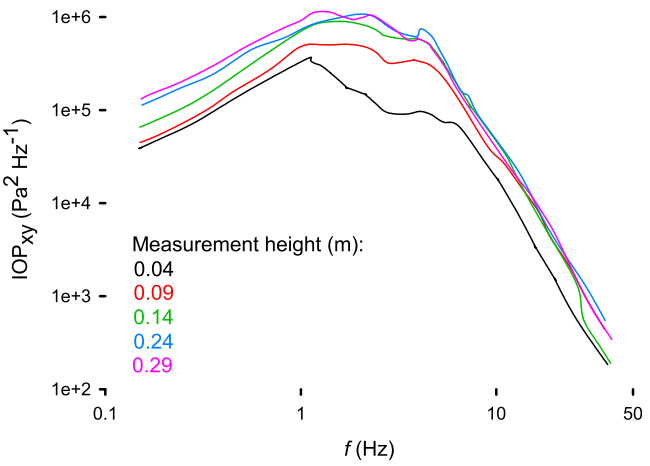

FIGURE 12 The incoherent-output power spectral density of pressure fluctuation induced by gas bubbles (or turbulence). Adapted from van der Schaaf et al.[49]

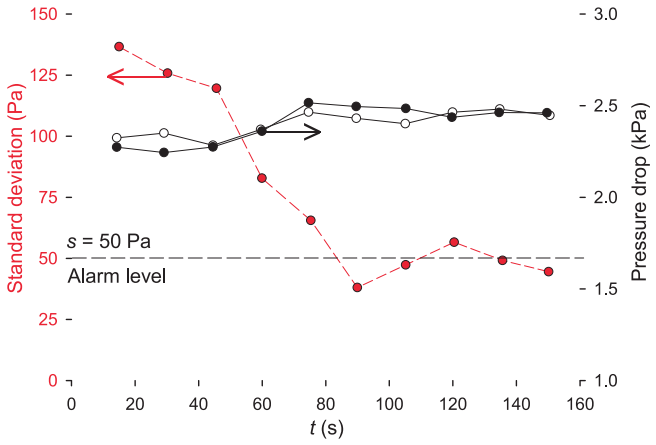

FIGURE 13 Standard deviation of pressure fluctuation and average pressure drop (full symbols = 0.04 to 0.44 m and empty symbols = 0.44 to 0.82 m) as a function of time. Reprinted from van Ommen et al.[20] with permission

representative and robust to outliers.[59] An inappropriate preparation protocol introduces an error. Pressure transducers are generally connected to a line that leads to a port in direct contact with a vessel.[51] Dynamic fluctuations in the line might interfere with the reading due to resonance and viscous damping. Shorter lengths minimize these phenomena. The analyses of low-frequency events require line lengths below 2.5 m. If a short line is impractical, the Bergh and Tijdeman model can be applied to calculate the optimal line.[51,60] The signal degrades due to snubbers, screens, and connecting lines between the tap and the transducer. The ideal line diameter is from 2 to 5 mm. Smaller diameters dampen the signal, whereas a larger diameter amplifies resonance and disturbs the hydrodynamics in the case of a line that is

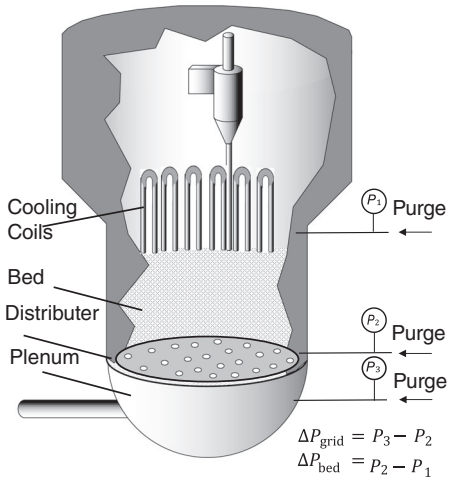

FIGURE 14 Pressure tap configuration to measure pressure drop across the plenum and measure ΔP in the fluidized bed to estimate bed density and bed height. The pressure taps operate at a sonic velocity and a purge mass flow rate of 1 kg s^{-1}

purged.[51] Fine grains, under strong agitation of uprising bubbles and gas, easily enter and contaminate and eventually clog the hose and pressure sensors. Covering the entrance with a fine wire mesh minimizes particle ingress while maintaining the signal integrity.[59] Charged particles developed over time also potentially clog probe openings. A constant gas purge to the sample port operating at sonic velocity is standard practice commercially but risks excessively perturbing experimental rigs. In small rigs, a flow rate of 0.5–1 ms^{-1} is appropriate for Geldart A particles, while 1–2 ms^{-1} is good for Geldart B particles.[25] Positioning probes flush to the wall minimizes disturbing the hydrodynamics. In large-scale beds, pressure waves caused by bubble breakup and formation propagate up to 50 cm away from its origin.[59] Therefore, the radial spacing of adjacent probes should not be greater than 1 m, if local hydrodynamic phenomena are interested. Flushing probes to the wall suffices for a smaller bed. It is unavoidable to place one or more probes inside large units, and intrusion disturbs the bed hydrodynamics. An optimal arrangement should be considered to reduce the number of probes to apply.[61] In the case of vigorous fluidization, plenum pressure measurements can be alternatives.[62] For applications in which global hydrodynamics events are not interesting, such as tracking bubbles, probes of differential sensors or two absolute sensors can be positioned between a minimal axial distance to eliminate global waves. Pressure probes are capable of detecting local hydrodynamic events, like waves at radial instances of 0.3–0.5 m at a gas velocity of 0.5 ms^{-1}. Probes flush to the wall are adequate for small beds, but to identify local phenomena in large beds, the probes must be less than 1 m apart, but this

intrusion may disturb the bed hydrodynamics. Measuring pressure in the plenum is an alternative in the case of vigorous fluidization.[62]

For gas–solid fluidized beds, sampling pressure fluctuations at frequencies of 20–40 Hz is sufficient, as the majority of hydrodynamic events occur at a rate below 10 Hz.[20,28] Electric pressure transducers sample at kilohertz, which is far in excess of the required rate to probe bubbling beds or avoid signal aliasing.

The sampling period depends on the application and analysis. We recommend 30 min for spectral and non-linear analyses. A series of 10 s is too short to characterize events occurring at 4–10 Hz.[20,63] Filtering is commonly applied to pre-treat the raw signal to exclude unnecessary components. For example, the Nyquist criterion recommends applying a low-pass filter at half the sampling frequency or lower. On the other hand, a high-pass filter with a low cut-off frequency (e.g., 0.1 Hz) removes slow trends.

4.2 | Selection of an electric pressure sensor

We select pressure sensors considering the environment, application, operators, and location.

4.2.1 | Sensors category

Absolute pressure measurements probe the temporal or spatial evolution of atmospheric pressure, such as elevation based on the atmospheric pressure variation with altitude, or the degree of vacuum during degassing. When measuring system pressure, absolute pressure sensors are appropriate only when the contribution from the barometric pressure is inconsequential. Relative pressure sensors (gauges) $P - P_{\text{atm}}$ are appropriate for measuring vacuum, for monitoring the level in vessels (hydrostatic pressure head), and for pipes, regulators, towers, and tanks. Differential pressure sensors are like relative pressure sensors but rather than the atmosphere, the second position is in the same process vessel so the sensor has two input channels, one on each side of the diaphragm, and the deformation corresponds to the pressure difference between the two inputs. They detect the buildup of filter cake for determining clean cycles, ΔP across orifices to evaluate flow rate, and, in fluidized beds, for monitoring hydrodynamics and identifying regime changes and particle size (Figure 14).

Special designs are required when one side of the process is dry (e.g., ambient conditions) and the other is a liquid. The alternative is to mount two absolute sensors with the the same internal electronic board to function as a differential sensor. However, the uncertainty, $\Delta_{\Delta P}$, is higher measuring two pressures compared to an integrated ΔP transducer. Consider a variable, f, that is a function of several factors, x_i[5]

$$f = f(x_1, x_2, ..., x_n). \tag{8}$$

The uncertainty, Δ_f, is

$$\Delta_f = \sqrt{\left(\frac{\partial f}{\partial x_1}\Delta_1\right)^2 + \left(\frac{\partial f}{\partial x_2}\Delta_2\right)^2 + \cdots + \left(\frac{\partial f}{\partial x_n}\Delta_n\right)^2} \tag{9}$$

For a function that is a sum or a difference of factors, $f = a_1x_1 - a_2x_2 + a_3x_3$, the uncertainty is

$$\Delta_f = \sqrt{(a_1x_1)^2 + (a_2x_2)^2 + ...(a_nx_n)^2} \tag{10}$$

The uncertainty in P, Δ_P, based on the difference in pressure P_1 and P_2, and $\Delta P = \Delta_{P1} = \Delta_{P2}$

$$\Delta P_{P1-P2} = \sqrt{2}\Delta_P \tag{11}$$

Assuming both the ΔP and P transducers have the same uncertainty at full scale (FS), $\Delta_{\Delta P}$ has a lower uncertainty by $\Delta_P/(1.4P)$.

4.2.2 | Sensors model

Piezoresistive, capacitive, and piezoelectric sensors are the most available electric sensors in the market. Although differentiating in the favourable measuring conditions, all these sensor models are robust, inexpensive, with a wide range of pressure measuring scale and operating temperature. Piezoresistive sensors are the most widely used type of pressure sensors, both in laboratory and industrial applications (Figure 3). They are inexpensive due to their simple yet durable construction. The voltage output is linearly proportional to the imposed pressure, with a fast response, typically < 1 ms. In addition, the measuring scale is sufficiently wide for most applications. However, due to the nature of resistive elements, leaks, or decay of the output could occur after long-time use, which potentially destabilizes the instrument. In its standard form, sensing elements are mounted onto the diaphragm, and the output becomes temperature dependent. Similarly, harsh environments, such as high temperature and over pressure, impair the signal. Besides, piezoresistive sensors require an external supply to power the Wheatstone circuit.

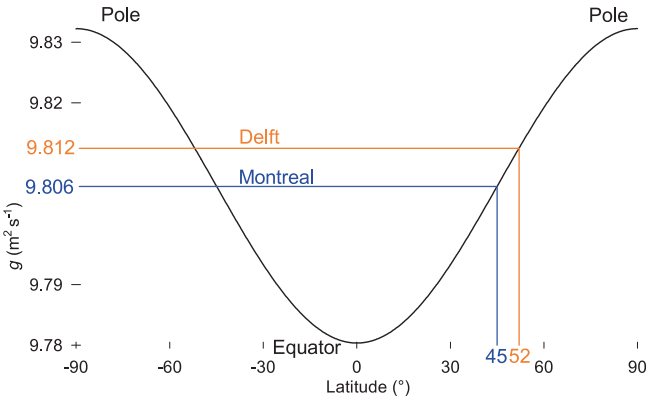

FIGURE 15 Gravitational constant, g, varies by 0.5% from pole to equator

The capacitive element is mechanically simple and robust, which produces a reproducible signal. The range of capacitive sensors is lower than that of piezoresistive sensors. In contrast, capacitive elements function under a much wider temperature range with less thermal drift, and tolerate short-term overpressure conditions (50 × FS). Given these advantages, they are ideal for both lower pressure measurements and harsh environments. Capacitive sensors also manifest low hysteresis, and the response time is in the order of milliseconds. The major disadvantage of capacitive sensors lies in the created capacitance, which is inversely proportional to the gap between the parallel electrodes. Therefore, it is inherently non-linear and sensitive to mechanical vibration. Besides, the permittivity of media between the electrodes varies slightly with ambient pressure and temperature. Applying a vacuum to the gap minimizes these errors. The sensors are robust and function up to 573 K,[64] but the electronic components limit the operating conditions.

Piezo crystals deform under pressure and are self-powered to create a charge. An amplifier, with an external power supply, converts charge to voltage and expands the output range. The amplifier electronics limit the operating temperature window. Similar to other electric sensors, piezoelectric elements are small with a fast dynamic response, that is, in the order of microseconds. Nevertheless, its structure is sensitive to mechanical vibration or acceleration.

Suitability, cost, physical dimensions, process connectors, accuracy rating, range, and response time are the features we consider when choosing a sensor. Accuracy is expressed as a percentage of FS, and, ideally, a sensor operates at 50% FS to maximize accuracy while minimizing damage due to over-pressure. High-resolution sensors capture minor—but critical—pressure fluctuations. While the sensors operate at a high temperature, the electronics limit the operation range from 248 to 353 K. Most sensors are threaded to mount easily in pipe and vessel wall ports. The metallic housing protects sensors from corrosion, overpressure, and high temperatures, but they require certification for service with explosive mixtures.

TABLE 2 Ranges and accuracy of calibration instruments (FS)[6]

Devices	Range	Accuracy at FS[a]
McLeod gauge	0.01–1 Pa	< 4%
Ionization gauge	0.02–10 Pa	< 6%
Deadweight tester	0.02–2 MPa	< 0.02%
U-tube manometer	0.1–15 MPa	< 0.01%
Vibrating cylinder gauge	< 0.35 MPa	0.005%
Au-Cr alloy gauge	> 700 MPa	1%

Abbreviation: FS, full scale.

4.3 | Calibration

4.3.1 | Choice of reference sensors

Pressure balances, piston gauges, manometers, and barometers are best for mid-pressure range (0.1–2 MPa) calibration, frequently encountered in laboratories, and they achieve an accuracy of ±0.1% FS. Manometers must be vertically aligned and operated isothermally. We recommend correcting for local gravity as it varies by 0.5% from the pole to the equator (Figure 15)[5]

$$g_\theta = 9.78\left(1 + 0.0053\sin^2\theta\right) \tag{12}$$

Barometeric pressure is highest at sea level and decreases with elevation, z (in m), in the troposphere according to

$$P = P_o(1 - 0.000\,0226z)^{5.25} \tag{13}$$

P varies with elevation, Z (in km), up to the thermosphere according to[5]:

$$P = P_o \exp\left(-0.114Z^{1.07}\right). \tag{14}$$

The barometric pressure in Quito (at 2850 m) is 70 kPa when the barometric pressure at sea level is 100 kPa, while in Calgary (at 1045 m), it is 88 kPa, and even at the top of Mont Royal in Montreal at 190 m, the pressure is 2% lower, $P = 97.7$ kPa (Equation (13)). Remember to check if weather services report barometric pressure as if it were at sea level, regardless of the elevation of the city.

For $P > 2$ MPa, electrical resistance sensors require manganin metal or gold–chromium alloys and a rigorous calibration. Electronic gauges are more expensive than Bourdon gauges and bellow, and their accuracy ranges from 0.1% to 0.5% FS. So the resolution of a gauge that measures 3000 MPa, is only 30 Pa. Regardless, the lowest recommended operating pressure is 10% FS.

McLeod gauges and micromanometers are appropriate for pressures from 0.02 to 10 Pa. Micromanometers consist of an inclined tube that is filled to amplify a reference pressure and minimize capillary effects and meniscus reading errors. This device is designed to accurately measure the pressure signal down to 0.1 Pa, but it requires accurate levelling. For pressures below 0.1 Pa, we apply a pressure divider—a series of orifices with an accurately tuned pressure ratio—that measures the upstream pressure with a McLeod gauge or micromanometer to compute the low-pressure gas at the sub-orifice. In addition, ionization gauges are also calibration references for ultra-low pressure in the range of 1×10^{-8}–100 Pa, but their accuracy is relatively poor (Table 2).

4.3.2 | Calibration frequency

Pressure sensors are typically calibrated during the manufacturing stage, and a recalibration is not required when are stored properly. After installation, we recommend calibrating sensors at least once a year. Applications in the pharmaceutical, biotechnology, and medical device sectors require calibration every 3–6 months to maintain optimized processes and minimize quality control failures. We categorize pressure sensor stability into several classes depending on the device type.[6] First-class sensors, such as resonant wire devices, ionization gauges, and high-pressure instruments, are very stable and unlikely to suffer drift over time. In addition, all forms of manometers are considered robust. Plastic deformation of the glass tube is likely to develop only after many years. Therefore, calibrating once a year is sufficient for first-class sensors, unless the device experiences a perturbance like a pressure burst.

Instruments consisting of an elastic element and a displacement transducer are classified in the second class. Devices of this type include diaphragms, bellows, and Bourdon tubes. We calibrate them on installation and recalibrate them annually. However, the signal drifts more than manometers in harsh environments or because of inappropriate handling and storage. Under these circumstances, calibrate them more frequently. The third class of instruments functions according to the thermal conductivity principle, including the thermocouple gauge, Pirani gauge, and thermistor gauge. The working parameters of these instruments vary with the nature of the gas being measured. Subsequently, they must be calibrated each time before commissioning.

4.3.3 | Calibration procedure

To calibrate an instrument requires that the reference instrument is more accurate in the target range. We connect the instruments to common lines and ramp the pressure through the desired range to compare the readouts. To minimize the chance of leaks, instal additional seals at the connection between the pressure source and the two instruments. Ideally, calibration should be carried out in-situ to avoid potential response delays and operational environment variations, such as temperature and humidity. Static calibration may induce charge leakage in electronic sensors, and the diaphragms stressed by an enduring, constant force over a long calibration time may reduce their working lifetime. A quasi-static calibration method applies to drop-weight devices, in which the piston is gradually pressed and peaks at its largest compression. The reference and operating sensors measure the dynamic response simultaneously,[65] including hysteresis, baseline offset (zero), and sensitivity error (e.g., Pa mV). Pressure bursts deform diaphragms that introduce all three errors.

Dynamic calibration applies when time response is essential, such as pressure fluctuation measurement and measurement synchronization. Transfer characteristics of pressure sensors, including relaxation time, natural frequency, damping ratio, and sensitivity, should be therefore determined.[66] We calibrate the frequency and time responses of the sensor against periodic and aperiodic pressure waves (e.g., a step signal), respectively.[67] Generation of these types of signals requires designated devices, such as shock tubes,[68] fast-opening valves,[68,69] and modulated weight or volume systems[69,70] In the calibration process of frequency response, sampling rate should follow the Nyquist theorem to avoid signal aliasing, and frequencies induced by the calibration setup itself could be excluded beforehand, for example, using Helmholtz resonance theory.

4.4 | Sampling

4.4.1 | Time series, the Hurst exponent

Harold Hurst collected hydrological data of the Nile basin (Egypt, Sudan, and East Africa) and developed a relationship that predicted if a series of sequential floods would

cluster around a high value followed by another high value ($0.5 < H < 1$) or alternate a high flood followed by a low flood ($0. < H < 0.5$).[33] When there is no correlation between the past and future events, H is equal to 0.5.[34]

This observation applies to pressure fluctuation in which we calculate the cumulative deviation from the mean of the time series ($\Delta_{\Delta P}$) in a time span k (N datapoints) from the pressure difference measured at a certain time (ΔP_k) and the average pressure difference of the whole time span selected ($\overline{\Delta P}_k$):

$$\begin{cases} \Delta_{\Delta P} = \sum_{k=1}^{N} \left(\Delta P - \overline{\Delta P}_k\right) \\ \overline{\Delta P}_k = \frac{1}{N} \sum_{k=1}^{N} \Delta P_k \end{cases} \tag{15}$$

From these two parameters, we calculate the standard deviation (s_k) of the timespan k.

$$s_k = \sqrt{\frac{1}{N} \sum_{k=1}^{N} (\Delta P_k - \Delta_{\Delta P})} \tag{16}$$

Also, for each time span (or sub interval), we calculate the range function (R_k):

$$R_k = \max(\Delta P_k) - \min(\Delta P_k) \tag{17}$$

The ratio between R_k and s_k is proportional to N, powered to a the Hurst exponent H:

$$\frac{R_k}{s_k} \propto N^H \tag{18}$$

For $H > 0.5$, the incoming data will have a positive autocorrelation and no correlation at $H = 0.5$ in the absence of anomalies and changing in fluidization regime, for a given dataset of differential pressure, H is greater than 0.5. For instance, with a Hurst number equal to 1 on the $\Delta_{\Delta P}$, a highly deterministic persistent phenomenon dominates, like the bubble motion. For low H ($H < 0.5$), it means that we are sampling more stochastic behaviour, like particle movement in dense beds.[35,36]

4.4.2 | Frequency domain, the Nyquist criterion

The Nyquist criterion assesses whether the sampling frequency of an instrument is adequate to observe a certain phenomenon in the domain of frequencies observed. It states that the sampling frequency must be at least twice the highest frequency contained in the signal, or information about the signal will be lost. Therefore, a sampling frequency of 2.4 Hz (or higher) is sufficient to characterize single-bubble regime or an exploding-bubble regime (Figure 8).[71] Nyquist published this work in 1928, with particular reference to telegraphy. The cost increases with increasing sampling rates but represents the data better. Lower sampling rates mean losses on digital information, but they are easier to achieve. In routine experiments, where we know the dominant frequency, the Nyquist criterion sets the lowest sample frequency to distinguish the target phenomenon.

4.5 | Sources of error and limitations

Although electronic pressure sensors are reliable, inappropriate installation and operation could induce error. Extreme working temperatures introduce faulty signals due to several electronic components that only function properly under a specified temperature working range, normally below 353 K. Normal pressure transducers are sensitive to temperature due to the expansion of internal parts caused by the rise in temperature and electronics. In order to measure a fluid at excessively high temperatures, for example, a fluidized bed combustor, the electric sensor should be installed far enough away from the hot surfaces and connected with heat-proof lines. Some pressure transducers operate at up to 973 K and even 1273 K (e.g., Kistler 6025A). Installing cooling elements is an alternative strategy.

The fluid being measured flows through a segment of metal shelled pipe first and cools down before entering the transducer. The larger the tube, the shorter the length is between the measuring nozzle and the pressure sensor. A lower than expected signal is due to leaks between the vessel and the transducer, plugged nozzle, or a physical damage to the sensing element. Clogging reduces the response time and dampens pressure fluctuations. Sensors exposed to mechanical vibration and shock can damage the housing, circuit, control boards, and diaphragms. Furthermore, gas entering the sample lines may resonate, introducing pressure flicks at the oscillation frequency. A simple solution is to relocate the sensor as remotely as possible from sources of shock and vibration or, depending on the installation, fabricate an ad hoc isolator for shock and vibration.

Zero-offset, or zero-unbalance, is one of the most common issues encountered in measurement. Once switched on, the pressure sensor outputs a non-zero signal without being subjected to any load of pressure. Such a zero-offset output is stable over time under the

measurement environments. It is associated with the unbalance in the Wheatstone bridge circuit caused by permanent deformation or rupture of the diaphragms. If the zero-offset is beyond a nominal tolerance (e.g, ±2%), operators must readjust it—trimming via a zero-adjustment resistor or a built-in zero-adjust pot.

Sudden bursts of pressure (shockwaves and spikes) damage sensors even when the pressure is within the permissible measuring range. The damage manifests itself as a faulty signal, hysteresis, sensitivity, or zero-off set. In the worst-case scenario, the pressure spikes break the diaphragm, resulting in leakage. Installing a snubber inside the measuring hose protects sensors from pressure spikes, but the trade-off is a dampened signal and lost information on high-frequency variations.

A pressure transducer converts the pressure load into an electrical signal that is susceptible to electromagnetic emissions or electrical disturbances. The-state-of-the-art transducers are fabricated to shield transducers from external EMI/radio frequency interference (RFI) disturbances; however, built-in designs sometimes are less effective to prevent disturbance generators from interfering. The output signal becomes noisy with tiny spikes. Hence, to minimize this noise, we place EMI/RFI far away from power lines, computers, walkie-talkies, and cell phones.

5 | CONCLUSIONS

Pressure, together with temperature, time, flow, and mass, is a basic physical property monitored in industrial operations and in the laboratory. The industry relies on pressure sensors to sound alarms and trigger interlocks to maintain a safe environment. However, several examples of measuring pressure incorrectly have precipitated catastrophes: 2005 Buncefield fire at an oil storage facility that was caused by a faulty level controller (and a faulty high-level switch); 2009 Air France Flight 447 crash due to the formation of ice crystals in a pitot tube that indicates air speed; and 2010 Macondo well blowout (Deepwater Horizon oil platform) related to poor interpretation of the downhole gauges. Pressure measurement continues to evolve and these disasters motivate companies to add redundancies to mitigate the chance for error. We expect the trend towards miniaturization to carry on (especially the transducers) and to see more options for sensors that function at extreme pressure and temperature. The accuracy and the precision of instruments depend on the application and the probe type. The main factors that affect the response of an instrument is an imperfect calibration, a wrong zeroing of the instrument, or an abnormal process condition that leads to the instrument's malfunction (high temperature or pressure bursts).

AUTHOR CONTRIBUTIONS

Kaiqiao Wu: Conceptualization; data curation; formal analysis; investigation; methodology; validation; visualization; writing – original draft; writing – review and editing. **Federico Galli:** Conceptualization; data curation; formal analysis; investigation; methodology; supervision; validation; visualization; writing – original draft; writing – review and editing. **Jacopo de Tommaso:** Conceptualization; data curation; formal analysis; investigation; methodology; validation; visualization; writing – original draft; writing – review and editing. **Gregory S. Patience:** Conceptualization; data curation; formal analysis; funding acquisition; investigation; methodology; project administration; resources; software; supervision; validation; visualization; writing – original draft; writing – review and editing. **J. Ruud van Ommen:** Conceptualization; data curation; formal analysis; funding acquisition; project administration; resources; supervision; validation; writing – original draft; writing – review and editing.

PEER REVIEW

The peer review history for this article is available at https://publons.com/publon/10.1002/cjce.24533.

DATA AVAILABILITY STATEMENT

All data will be made available to anyone that requests it from the authors.

ORCID

Gregory S. Patience https://orcid.org/0000-0001-6593-7986

REFERENCES

[1] E. Gassmann, *Chem. Eng. Prog.* **2014**, *110*, 637.
[2] C. Gaspari, E. dos Reis, in *Proc COBEM 2007 19th Int. Congress Mechanical Engineering* Brasilia, Brazil **2007**, pp. 1–8.
[3] G. S. Patience, *Can. J. Chem. Eng.* **2018**, *96*, 2312.
[4] H. T. Bi, *Chem. Eng. Sci.* **2007**, *62*, 3473.
[5] G. S. Patience, *Experimental Methods and Instrumentation for Chemical Engineers*, 2nd ed., Elsevier, Amsterdam, Netherlands **2017**.
[6] A. S. Morris, R. Langari, *Measurement and Instrumentation*, 2nd ed., Academic Press, Boston, MA **2016**, p. 463.
[7] L. Yanhua, Y. Hongyan, W. Jinku, *Vacuum* **2012**, *86*, 903.
[8] J. Fraden, *Handbook of Modern Sensors: Physics, Designs, and Applications*, 4th ed., Springer, New York **2010**, p. 375 Ch.4.
[9] Why you need Millivolt Output Pressure Transducers? www.eastsensor.com/blog/needmillivolt-output-pressure-transducers (accessed: July 2007).

[10] Pressure Sensors: The Design Engineer's Guide, www.avnet.com/wps/portal/abacus/solutions/technologies/sensors/pressure-sensors (accessed: October 2021).
[11] Pressure Transducers and Transmitters, www.omega.nl/prodinfo/pressure-transducers.html (accessed: October 2021).
[12] T. Gu, F. Shang, D. Kong, C. Xu, *Rev. Sci. Instrum.* **2019**, *88*, 055111.
[13] J. F. Davidson, D. Harrison, J. R. F. Guedes de Carvalho, *Annu. Rev. Fluid Mech.* **1977**, *9*, 55.
[14] E. R. Gilliland, *AIChE J.* **1964**, *10*, 783.
[15] J. van der Schaaf, J. C. Schouten, C. M. van den Bleek, *Powder Technol.* **1998**, *95*, 220.
[16] A. Baskakov, V. Tuponogov, N. Filippovsky, *Powder Technol.* **1986**, *45*, 113.
[17] H. Kage, M. Agari, H. Ogura, Y. Matsuno, *Adv. Powder Technol.* **2000**, *11*, 459.
[18] L. T. Fan, T.-C. Ho, S. Hiraoka, W. P. Walawender, *AIChE J.* **1981**, *27*, 388.
[19] J. Werther, *Powder Technol.* **1999**, *102*, 15.
[20] J. R. van Ommen, S. Sasic, J. van der Schaaf, S. Gheorghiu, F. Johnsson, M.-O. Coppens, *Int. J. Multiphase Flow* **2011**, *37*, 403.
[21] F. Johnsson, R. Zijerveld, J. C. Schouten, C. M. van den Bleek, B. Leckner, *Int. J. Multiphase Flow* **2000**, *26*, 663.
[22] J. Xiang, Y. Zhang, Q. Li, *Particuology* **2019**, *47*, 1.
[23] L. Dong, Y. Zhao, L. Peng, J. Zhao, Z. Luo, Q. Liu, C. Duan, *Particuology* **2015**, *21*, 146.
[24] X. Cong, X. Guo, H. Lu, X. Gong, K. Liu, X. Sun, K. Xie, *Chem. Eng. Sci.* **2013**, *101*, 303.
[25] J. van Ommen, R.-J. de Korte, C. M. van den Bleek, *Chem. Eng. Process.* **2004**, *43*, 1329.
[26] C. Felipe, S. Rocha, *Powder Technol.* **2007**, *174*, 104.
[27] C. Sobrino, S. Sánchez-Delgado, N. García-Hernando, M. de Vega, *Chem. Eng. Res. Des.* **2008**, *86*, 1236.
[28] H. Bi, N. Ellis, I. Abba, J. Grace, *Chem. Eng. Sci.* **2000**, *55*, 4789.
[29] H. He, X. Lu, W. Shuang, Q. Wang, Y. Kang, L. Yan, X. Ji, G. Luo, H. Liu, *Particuology* **2014**, *16*, 178.
[30] J. Xu, X. Bao, W. Wei, G. Shi, S. Shen, H. Bi, J. Grace, C. Lim, *Powder Technol.* **2004**, *140*, 141.
[31] M. Bartels, B. Vermeer, P. J. T. Verheijen, J. Nijenhuis, F. Kapteijn, J. R. van Ommen, *Ind. Eng. Chem. Res.* **2009**, *48*, 3158.
[32] A. V. Oppenheim, L. S. Willsky, S. H. Nawab, *Signals and Systems*, Pearson Education Ltd., New York **2014**.
[33] H. E. Hurst, *Proceedings of the Institution of Civil Engineers* **1956**, *5*, 519.
[34] H. E. Hurst, *Trans. Am. Soc. Civ. Eng.* **1951**, *116*, 770.
[35] H. Sedighikamal, R. Zarghami, *Part. Sci. Technol.* **2013**, *31*, 51.
[36] C. L. Briens, L. A. Briens, J. Hay, C. Hudson, A. Margaritas, *AIChE J.* **1997**, *43*, 1904.
[37] J. Stringer, in *10th Int. Conf. Fluidized Bed Combustion,* ASME, New York **1989**, pp. 265–272.
[38] C. M. van den Bleek, J. C. Schouten, *Chemical Engineering Journal and the Biochemical Engineering Journal* **1993**, *53*, 75.
[39] F. Takens, *Dynamical Systems and Turbulence, Warwick*, Vol. 1981, Springer, Cham, Switzerland **1980**, p. 366.
[40] J. C. Schouten, F. Takens, C. M. van den Bleek, *Phys. Rev. E* **1994**, *49*, 126.
[41] Clarivate Analytics Web of Science™ Core Collection, apps.webofknowledge.com (accessed: December 2021).
[42] N. J. van Eck, L. Waltman, *Scientometrics* **2010**, *84*, 523.
[43] M. M. Abu-Omar, K. Barta, G. T. Beckham, J. S. Luterbacher, J. Ralph, R. Rinaldi, Y. Roman-Leshkov, J. S. M. Samec, B. F. Sels, F. Wang, *Energy Environ. Sci.* **2022**, *14*, 262.
[44] Y. Yang, Y. Yang, Y. Cao, X. Wang, Y. Chen, H. Liu, Y. Gao, J. Wang, C. Liu, W. Wang, J.-K. Yu, D. Wu, *Chem. Eng. J.* **2021**, *403*, 126431.
[45] W. Yang, D. Pudasainee, R. Gupta, W. Li, B. Wang, L. Sun, *Fuel* **2021**, *213*, 106657.
[46] A. Etminan, Y. S. Muzychka, K. Pope, *Can. J. Chem. Eng.* **2022**, *100*, 325.
[47] B. Harimi, M. Masihi, M. H. Ghazanfari, *Can. J. Chem. Eng.* **2021**, *99*, S212.
[48] Z. Ding, S. S. Tiwari, M. Tyagi, K. Nandakumar, *Can. J. Chem. Eng.* **2022**, *100*, 405.
[49] J. van der Schaaf, J. C. Schouten, F. Johnsson, C. M. van den Bleek, *Int. J. Multiphase Flow* **2002**, *28*, 865.
[50] D. Argyriou, H. List, R. Shinnar, *AIChE J.* **1971**, *17*, 122.
[51] J. R. van Ommen, J. C. Schouten, M. L. M. van der Stappen, C. M. van den Bleek, *Powder Technol.* **1999**, *106*, 199.
[52] J. Xiang, Q. Li, Z. Tan, Y. Zhang, *Chem. Eng. Sci.* **2017**, *174*, 93.
[53] M. Bartels, J. Nijenhuis, F. Kapteijn, J. Ruud van Ommen, *Powder Technol.* **2010**, *202*, 24.
[54] C. E. Davies, A. Carroll, R. Flemmer, *Powder Technol.* **2008**, *180*, 307.
[55] O. Sitnai, *Chem. Eng. Sci.* **1982**, *37*, 1059.
[56] K. Svoboda, J. Čermák, M. Hartman, J. Drahoš, K. Selucký, *AIChE J.* **1984**, *30*, 513.
[57] J. van der Schaaf, J. R. van Ommen, F. Takens, J. C. Schouten, C. M. van den Bleek, *Chem. Eng. Sci.* **2004**, *59*, 1829.
[58] R. C. Brown, E. Brue, *Powder Technol.* **2001**, *119*, 68.
[59] J. R. van Ommen, R. F. Mudde, *Int. J. Chem. React. Eng.* **2008**, *6*, R3.
[60] H. Bergh, H. Tijdeman, *Theoretical and Experimental Results for the Dynamic Response of Pressure Measuring Systems* (Report No. NLR-TR F.238), **1965**. https://doi.org/10.13140/2.1.4790.1123
[61] J. R. van Ommen, J. van der Schaaf, J. C. Schouten, B. G. van Wachem, M. O. Coppens, C. M. van den Bleek, *Powder Technol.* **2004**, *139*, 264.
[62] H. Kage, N. Iwasaki, H. Yamaguchi, Y. Matsuno, *J. Chem. Eng. Jpn.* **1991**, *24*, 76.
[63] J. Matthew *PhD Thesis*, Chemical Engineering, Virginia Polytechnic Institute and State University (Blacksburg, VA) **2000**.
[64] B. R. Upadhyaya, R. T. Wood, *in Encyclopedia of Nuclear Energy*, (Eds: E. Greenspan), Elsevier, Oxford **2021**, pp. 373.
[65] T. Gu, F. Shang, D. Kong, C. Xu, *Rev. Sci. Instrum.* **2019**, *90*, 055111.
[66] R. F. R. Theodoro, M. L. C. da Costa Reis, C. D. A. Souto, E. Barros, *Measurement* **2016**, *88*, 238.
[67] ISA-37.16.01-2002 A guide for the dynamic calibration of pressure transducers, https://www.isa.org/products/isa-37-16-01-2002-a-guide-for-the-dynamic-calibrat (accessed: March 2022).
[68] A. C. G. C. Diniz, A. B. Oliveira, J. Vianna, F. Neves, in *XVIII IMEKO World Congress Metrology*, IMEKO, Rio de Janeiro **2006**, pp. 17–22.

[69] A. S. Melaaen *Master's Thesis*, Norwegian University of Science and Technology (Trondheim, Norway) **2017**.
[70] Y. Durgut, O. Ganioglu, B. Aydemir, A. Turk, R. Yilmaz, A. Hamarat, E. Bagci, in *19th Int. Congress Metrology*, EDP Sciences, Les Ulis, France **2019**, 27009.
[71] R. V. L. Hartley, *Bell Syst. Tech. J.* **1928**, *7*, 535.

How to cite this article: K. Wu, F. Galli, J. de Tommaso, G. S. Patience, J. R. van Ommen, *Can. J. Chem. Eng.* **2022**, 1. https://doi.org/10.1002/cjce.24533